ACUSTICA · acta acustica
Vol. 84 (1998) 289 – 300

Vertical Rail Vibrations: Parametric Excitation

Anders Nordborg*
The Marcus Wallenberg Laboratory for Sound and Vibration Research, Royal Institute of Technology, S-10044 Stockholm, Sweden

Summary
Green's function of a periodically supported, infinite beam describes rail responses to moving loads, where the excitation may depend on roughnesses, varying rail receptance together with vehicle weight including the wheel inertia. The frequency domain solution of the linear differential equation governing rail response, yields a simple, comprehensive and computation efficient tool in sound/vibration optimising track constructions. A railway wheel traversing a sleeper-supported rail 'sees' a varying receptance downwards. This parametric excitation, causing the wheel to move up and down at the sleeper-passing frequency (50–100 Hz), is a source of low frequency structure-borne sound and vibration, with implications for nearby buildings, passanger compartments and radiation from railway bridges. Coincidence, between the sleeper-passing frequency and wheel-ballast resonance, results in great amplitudes. A comparison with long-scale 'roughness' excited rail vibrations shows that parametric excitation dominates below the wheel-ballast resonance, assuming the same 'roughness' amplitude as the static deflection variation. The dynamic contact force caused by short-scale roughnesses fluctuates through the sleeper bays, with stiff pads providing an extra excitation mechanism around the pinned-pinned frequency (~ 1000 Hz). Softer pads may lower vibration levels at the sleeper-passing frequency and around the pinned-pinned frequency; at the same time, however, other levels may increase.

PACS no. 43.40.At, 43.40.Cw, 43.50.Lj

1. Introduction

A railway wheel traversing a sleeper-supported rail 'sees' a varying receptance downwards. This parametric excitation, causing the wheel to move up and down at the sleeper-passing frequency, is a source of low frequency structure-borne sound and vibration, with implications for nearby buildings, passanger compartments and radiation from railway bridges. A great number of measurements, e.g. in [1] by Wettschureck and Hauck, illustrate its significance.

Auersch [2] estimates the response of a railway wheel to parametric excitation; ground vibration measurements from the ICE verify the predictions. Heckl [3, 4] studies the bending wave equation of a rail modelled as an Euler-beam on a varying foundation stiffness. He expands the stiffness as a series with a constant plus a sinusoidally varying term, assuming small variations; he also expands the deflection variation under a concentrated moving force as a series with a decaying order of magnitude, resulting in a system of coupled differential equations, which may be solved iteratively. Ripke [5] clearly demonstrates the Doppler effect, including force modulation due to varying rail receptance, for moving harmonic force excitations, with time-step integration. Frýba's monograph [6] deals with vibrations of mechanical structures subjected to various moving loads. He gives a thorough review of the subject from the beginning of this century to the early 70s. Knothe's and Grassie's review [7] reaches to the beginning of the 90s. Early works were done by Timoshenko [8], Inglis [9] and Dörr [10, 11].

Received 21 December 1995,
accepted 23 December 1997.

* Current address: ABB Corporate Research, S-72178 Västerås, Sweden

The present paper[1] picks ideas from Ilias and Knothe [14] and Kisilowski *et al.* [15] when including the effects of the forward velocity of the wheel. Green's function $G_\omega(x|x_0)$ together with the Fourier transform of the excitation force by superposition produces solutions to moving load problems. The solution, a Fourier transform of G, $\hat{G}_\omega[(\omega_0-\omega)/v; x_0]$, where $\hat{}$ denotes Fourier transformation in the space variable x, is exact and analytic, displaying for instance a frequency Doppler shift at a fixed observation point x_0 of the rail. Fourier transforming $\hat{G}_\omega[(\omega_0-\omega)/v; x_0]$ back to time, substituting vt for x_0 and transforming back to frequency again, yields an expression for the velocity dependent response. In the time domain, the force has a static part, $M_{\text{veh}}g$, corresponding to the weight of the vehicle, while the dynamic part represents the acceleration, $\mathrm{d}^2y(x,t)/\mathrm{d}t^2$, of the wheel with mass M_{w}. A little algebra gives an infinite system of equations, in matrix form $\boldsymbol{x} = \boldsymbol{A}\boldsymbol{x} + \boldsymbol{b}$, where vector $\boldsymbol{x}$ contains Fourier coefficients of the response. The inhomogeneity $\boldsymbol{b}$ of the discretised integral equation, or the driving force of the system, corresponds to the static deflection variation through a sleeper span caused by the weight of the vehicle, $M_{\text{veh}}g$. The term $\boldsymbol{A}\boldsymbol{x}$ corresponds to the dynamic part of the interaction force.

Vertical deflection reaches a maximum when the sleeper-passing frequency coincides with the wheel-ballast resonance. A change of track parameters is an efficient way of reducing parametrically excited vibrations, as shown by a number of calculations, of which the following are suggested: increase the receptance of the track, either through pads or ballast; shorten sleeper spacings; and select a stiffer and heavier rail. A comparison between parametric excita-

[1] This work can also be found in the thesis [12]. Parts were presented at DAGA 94 [13].

ACUSTICA · acta acustica
Vol. 84 (1998)

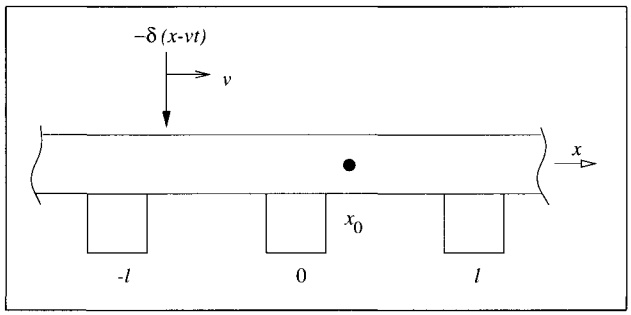

Figure 1. Excitation by a moving harmonic force.

tion of the rail and 'corrugation' excitation, demonstrates that parametric excitation is the more important in the frequency (velocity) range below the wheel-ballast resonance, so the lower the frequency the greater the importance of parametric excitation. The wheel, however, responds equally to 'roughness' as to receptance variation, in the whole frequency range of interest.

A moving wheel model includes the effect of forward velocity and rail-sleeper periodicity on the noise and structure-borne sound production. At the sleeper-passing frequency f_s this produces ground-borne vibrations and compartment noise; around the pinned-pinned frequency f_{pp} air-borne noise. The force modulation of roughness excitations is an extra excitation mechanism, which is significant provided that stiff pads are used. In changing from stiff to soft pads, the vibration level generally increases, except around the pinned-pinned frequency where it decreases.

2. Theory

2.1. Moving Load Excitation

2.1.1. Green's Function Application

Application of Green's function forms the solution to moving load problems. If the general problem

$$\mathrm{L}Y = F,$$

where the differential operator L is defined in a companion paper [16], it is shown in the thesis [12] that the unique solution

$$Y(x_0,\omega) = \int_{-\infty}^{\infty} G_\omega(x|x_0)F(x,\omega)\,\mathrm{d}x, \qquad (1)$$

where $F = F(x,\omega)$ is the Fourier transform of the force $f(x,t)$ exciting the rail; i.e. by using Green's function rail response to any Fourier transformed excitation is calculated. Equation (1) assumes the reciprocity principle of Green's function, i.e. if source and observation points are interchanged, $G_\omega(x|x_0) = G_\omega(x_0|x)$. From now on, x denotes the source point and x_0 the observation point. For a fixed point excitation, i.e. $f(x,t) = \delta(x-x_0)\mathrm{e}^{-\mathrm{i}\omega_0 t}$ and $F(x,\omega) = \delta(x-x_0)\delta(\omega-\omega_0)$, the rail has a response at the excitation circular frequency $\omega = \omega_0$ only, $Y = G_\omega\delta(\omega-\omega_0)$.

2.1.2. Moving Harmonic Force Excitation

Fix Point Response A moving, harmonically oscillating unit force, with velocity v and circular frequency ω_0, approaches, from $x = -\infty$, position x_0 and disappears at $x = +\infty$ (Figure 1). Then, the excitation $f(x,t) = \delta(x-vt)\mathrm{e}^{-\mathrm{i}\omega_0 t} = \frac{1}{v}\delta(t-1/v)\mathrm{e}^{-\mathrm{i}\omega_0 t}$; the Fourier transform becomes

$$\begin{aligned} F(x,\omega) &= \frac{1}{2\pi}\int_{-\infty}^{\infty}\frac{1}{v}\delta\left(t-\frac{x}{v}\right)\mathrm{e}^{-\mathrm{i}\omega_0 t}\mathrm{e}^{\mathrm{i}\omega t}\,\mathrm{d}t \\ &= \frac{1}{2\pi v}\mathrm{e}^{-\mathrm{i}\frac{\omega_0-\omega}{v}x}. \end{aligned} \qquad (2)$$

To calculate the response at x_0, use (1),

$$\begin{aligned} Y(x_0,\omega) &= \frac{1}{2\pi v}\int_{-\infty}^{\infty} G_\omega(x|x_0)\mathrm{e}^{-\mathrm{i}\frac{\omega_0-\omega}{v}x}\mathrm{d}x \\ &= \frac{1}{2\pi v}\hat{G}_\omega\left(\frac{\omega_0-\omega}{v};x_0\right). \end{aligned} \qquad (3)$$

The Fourier transform in the x direction of Green's function, $\hat{G}_\omega$, is evaluated analytically in Appendix A1. The factor $\kappa^2 - k^2 = [(\omega_0-\omega)/v]^2 - (\omega/c_B)^2$ in the denominator of $\hat{G}_\omega$, where c_B is the bending wave velocity, represents a Doppler shift at the observation point x_0, since for $\kappa^2 - k^2 \simeq 0$, $\omega \simeq \omega_0(1\pm M)^{-1}$, where $M = v/c_B \ll 1$ ($c_{B,\min} \simeq 500$ m/s and $v \leq 100$ m/s for normal train/track systems). Thus, the frequency shift $f \simeq f_0 \pm v/\lambda_B$, λ_B being bending wavelength. The factor $\kappa^2 - k^2$ becomes minute near the critical speed, e.g. if $\omega_0 = 0$ and $v \to c_B$, so that the response amplitude increases very much indeed. In the low velocity limit ($v \to 0$), the energy of the response (see Appendix A2)

$$2\pi\int_{-\infty}^{\infty}|Y(x_0,\omega)|^2\,\mathrm{d}\omega \to \frac{1}{v}\int_{-\infty}^{\infty}|G_{\omega_0}(x|x_0)|^2\,\mathrm{d}x.$$

This approximation holds for all realistic train speeds, since $M \ll 1$.

Moving Point Response Moving point response $y_v(t)$ is found making the substitution $x_0 = vt$ in the time-domain. The periodicity of the structure modulates the harmonic excitation force, suggesting the form (see [14, 15]):

$$y_v(t) = \sum_{n=-\infty}^{\infty} a_n(\omega_0)\mathrm{e}^{-\mathrm{i}(\omega_0+\Omega_n)t}, \qquad (4)$$

where sleeper-passing circular frequency and harmonics, $\Omega_n = 2\pi n/T$ with $T = l/v$. This is also a consequence of Floquet's theory seeking a solution of the form $y_v(t) = P(t,\omega_0)\mathrm{e}^{\mathrm{i}\gamma t}$, where γ, the characteristic exponent, is the phase shift of the force during one period T, and P is periodic, $P(t+T,\omega_0) = P(t,\omega_0) = \sum_{n=-\infty}^{\infty} a_n(\omega_0)\mathrm{e}^{-\mathrm{i}\Omega_n t}$. The requirement $y_v(t+T) = y_v(t)\mathrm{e}^{-\mathrm{i}2\pi T/T_0}$, where $T_0 = 2\pi/\omega_0$, fixes $\gamma = -\omega_0$, and (4) is proved.

The Fourier coefficients a_n are obtained through the inverse transform of $Y(x_0,\omega)$, (3), with the substitution of vt for x_0:

$$y_v(t) = \sum_{n=-\infty}^{\infty} a_n(\omega_0)\mathrm{e}^{-\mathrm{i}(\omega_0+\Omega_n)t} \qquad (5)$$
$$= \frac{1}{2\pi v}\int_{-\infty}^{\infty} \hat{G}_\omega\left(\frac{\omega_0-\omega}{v};vt\right)\mathrm{e}^{-\mathrm{i}\omega t}\,\mathrm{d}\omega,$$

so that

$$a_n(\omega_0) = \frac{1}{T}\int_0^T \frac{1}{2\pi v}\int_{-\infty}^{\infty} \hat{G}_\omega\left(\frac{\omega_0-\omega}{v};vt\right) \cdot \mathrm{e}^{\mathrm{i}(\omega_0-\omega)t}\,\mathrm{d}\omega\,\mathrm{e}^{\mathrm{i}\Omega_n t}\,\mathrm{d}t. \qquad (6)$$

In calculating $\lim_{v\to 0} a_n(\omega_0)$, the order of taking $\lim_{v\to 0}$ and $\int \mathrm{d}\omega$ may be interchanged (see Appendix A2). With the substitutions $\kappa = (\omega_0-\omega)/v$, $x_0 = vt$, $l = vT$ and $k_n = \Omega_n/v$,

$$\lim_{v\to 0} a_n(\omega_0) = \frac{1}{l}\int_0^l \frac{1}{2\pi}\int_{-\infty}^{\infty} \hat{G}_{\omega_0}(\kappa;x_0) \cdot \mathrm{e}^{\mathrm{i}\kappa x_0}\,\mathrm{d}\kappa\,\mathrm{e}^{\mathrm{i}k_n x_0}\,\mathrm{d}x_0.$$

Thus, for v small,

$$a_n(\omega_0) \simeq \frac{1}{l}\int_0^l G_{\omega_0}(x_0|x_0)\mathrm{e}^{\mathrm{i}k_n x_0}\,\mathrm{d}x_0. \qquad (7)$$

This approximation is valid for all practical train speeds, being much less than the lowest bending wave velocity, shown by Ilias and Knothe [14], in studying velocity-dependence of moving harmonic force response, though with less straightforward calculations than here. Moreover, only the three Fourier coefficients a_0 and $a_{\pm 1}$ need be considered to describe the rail motion in the frequency range 0–2000 Hz [14], because $a_n \to 0$ rapidly as $n \to \pm\infty$ [$a_n = \mathcal{O}(n^{-4})$ as $n \to \pm\infty$ since $G_\omega^{(iv)}(x|x)$ is absolutely integrable, except for a few isolated step discontinuities of $G_\omega'''(x|x)$]. To sum, this analysis shows that a_n, defined by (4) and (6), are the Fourier coefficients for the receptance variation (with unit m/N) through a sleeper span, taking the dependence (though small) of the velocity v into account.

A certain relation exists between $a_n(\omega_0)$ and the Fourier coefficients of an expansion of (3), $g_j(\omega,\omega_0)$, if ω_0 is a multiple of the fundamental circular frequency. That is $\omega_0 = \Omega_m$ to guarantee periodicity. Then, the vibrational response one period ahead of x, $y(x+l,t)$, and the vibrational response at x, $y(x,t)$, are related through $y(x+l,t) = y(x,t-l/v)$, because of the system periodicity. Fourier transforming this relation,

$$Y(x+l,\omega) = \frac{1}{2\pi}\int_{-\infty}^{\infty} y\left(x,t-\frac{l}{v}\right)\mathrm{e}^{\mathrm{i}\omega t}\,\mathrm{d}t,$$

and changing variable of integration to $t' = t - l/v$ results in the equality $Y(x+l,\omega) = Y(x,\omega)\mathrm{e}^{\mathrm{i}\frac{\omega}{v}l}$. According to the Floquet theory, define $Y(x,\omega)$ as a periodic function $P(x+l,\omega) = P(x,\omega)$ times a phase factor $\mathrm{e}^{\mathrm{i}\gamma x}$, $Y(x,\omega) = P(x,\omega)\mathrm{e}^{\mathrm{i}\gamma x}$. It then follows that $\gamma = \omega/v$, so that—as P can be expanded into a Fourier series—

$$Y(x,\omega) = \sum_{n=-\infty}^{\infty} \chi_n(\omega)\mathrm{e}^{-\mathrm{i}(k_n-\frac{\omega}{v})x}, \qquad (8)$$

where $k_n = 2\pi n/l$. This expression is used in Sec. 2.2.1.

Now, (8) and (3), where $g_j(\omega,\Omega_m)$ is substituted for $\chi_n(\omega)$, yield the Fourier expansion of the Floquet solution:

$$Y(x_0,\omega) = \frac{1}{2\pi v}\hat{G}_\omega\left(\frac{\Omega_m-\omega}{v};x_0\right) = \sum_{j=-\infty}^{\infty} g_j(\omega,\Omega_m)\mathrm{e}^{-\mathrm{i}(k_j-\frac{\omega}{v})x_0}.$$

Substitute this series, with $x_0 = vt$, into (6); $\omega_0 = \Omega_m$ as mentioned above. Then, (6) takes the form

$$a_n(\Omega_m) = \sum_{j=-\infty}^{\infty}\int_{-\infty}^{\infty} g_j(\omega,\Omega_m)\,\mathrm{d}\omega \cdot \frac{1}{T}\int_0^T \mathrm{e}^{\mathrm{i}\omega-j+m+n\,t}\,\mathrm{d}t.$$

Since the last integral is zero, except for $j = n+m$ when it equals T,

$$a_n(\Omega_m) = \int_{-\infty}^{\infty} g_{n+m}(\omega,\Omega_m)\,\mathrm{d}\omega, \qquad (9)$$

providing an alternate expression to (6) for computing the velocity dependent point receptance (when $\omega_0 = \Omega_m$).

2.2. Parametric Excitation

2.2.1. Wheel Inertia Forces

For simplicity, assume first that the vehicle is a rigid mass M_w only, so that the vertical vehicle receptance at the contact point is $\alpha_\mathrm{veh} = -1/M_\mathrm{w}\omega^2$ for simple harmonic motion. (The receptance of the wheel is the vertical displacement Y as caused by a harmonic contact force F, $\alpha_\mathrm{veh} = Y/F$.) The rail receptance is periodic in the x-direction, because of the periodic supports, and can thus be written as the Fourier series $\alpha_\mathrm{r} = \sum_{n=-\infty}^{\infty} a_n\mathrm{e}^{\mathrm{i}k_n x}$, where $k_n = 2\pi n/l$, and the coefficients a_n are defined by (4). At the end of this subsection (2.2.1), generalise the derived interaction force, F, to a vehicle with any mass, M_veh, and vertical receptance at the contact point, α_veh, including e.g. a contact spring or wheel resonances.

Rail and wheel have the same vertical deflection at the contact point. Thus, the rail is subjected to the inertia force of the wheel (Figure 2),

$$f(x,t) = M_\mathrm{w}\left[-\frac{\mathrm{d}^2 y(x,t)}{\mathrm{d}t^2} - g\right]\delta(x-vt), \qquad (10)$$

ACUSTICA · acta acustica
Vol. 84 (1998)

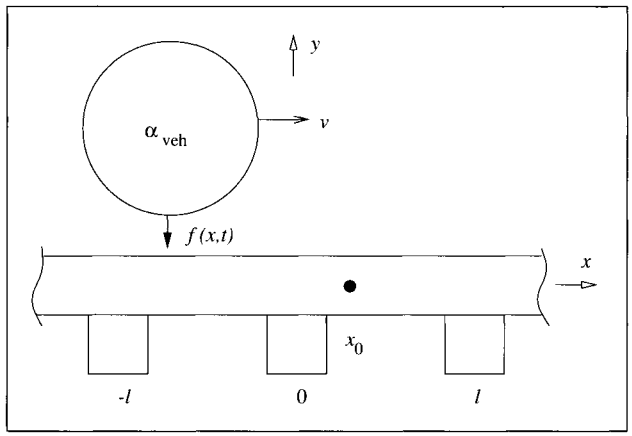

Figure 2. Excitation of the rail through wheel inertia forces.

where g is the constant of gravity. The variables x and t are related, $x = vt$, through the delta function $\delta(x - vt)$, so that the total acceleration is

$$\frac{\mathrm{d}^2 y(x,t)}{\mathrm{d}t^2} = \frac{\partial^2 y(x,t)}{\partial t^2} + 2v\frac{\partial^2 y(x,t)}{\partial x \partial t} + v^2\frac{\partial^2 y(x,t)}{\partial x^2}. \quad (11)$$

The second term on the right represents the Coriolis force, and the third term the centripetal acceleration.

Before proceeding with the derivation of the Fourier transform F of the force f, express the Fourier transform of the response at the fixed point x, $Y(x,\omega)$, as a series, taking into account that $Y(x,\omega)$ is a Floquet solution; we also need a relation between the matching Fourier coefficients χ_n and the Fourier coefficients x_n for the solution at the moving point $x = vt$. These expressions are of later use.

The form $Y(x,\omega)$ takes in (8) applies also here, for the same reasons. Periodicity implies that the response at the moving point $x = vt$ is

$$y_v(t) = \sum_{n=-\infty}^{\infty} x_n \mathrm{e}^{-\mathrm{i}\Omega_n t}, \quad (12)$$

where $\Omega_n = 2\pi v n/l$, and x_n are the unknowns to be found (do not confuse x_n with a space coordinate). Now, derive the relation between $\chi_n(\omega)$ and x_n. Start with the inverse Fourier transform,

$$y(x,t) = \int_{-\infty}^{\infty} Y(x,\omega)\mathrm{e}^{-\mathrm{i}\omega t}\,\mathrm{d}\omega,$$

and substitute (8) for Y,

$$y(x,t) = \sum_{n=-\infty}^{\infty}\int_{-\infty}^{\infty} \chi_n(\omega)\mathrm{e}^{-\mathrm{i}(k_n - \frac{\omega}{v})x}\mathrm{e}^{-\mathrm{i}\omega t}\,\mathrm{d}\omega.$$

Then put $x = vt$, $y(vt,t) = y_v(t)$, to obtain

$$y_v(t) = \sum_{n=-\infty}^{\infty}\int_{-\infty}^{\infty} \chi_n(\omega)\,\mathrm{d}\omega\,\mathrm{e}^{-\mathrm{i}\Omega_n t},$$

where $\Omega_n = k_n v$. Combine this equation with (12), end up with

$$x_n = \int_{-\infty}^{\infty} \chi_n(\omega)\,\mathrm{d}\omega, \quad (13)$$

which is a relation similar to that in (9).

Continue with the derivation of the Fourier transform of the exciting force F. Rewrite (11) by the inverse Fourier transform,

$$\frac{\mathrm{d}^2 y(x,t)}{\mathrm{d}t^2} = \int_{-\infty}^{\infty}\Big[-\omega_1^2 Y(x,\omega_1) - 2v\mathrm{i}\omega_1 Y'(x,\omega_1) + v^2 Y''(x,\omega_1)\Big]\mathrm{e}^{-\mathrm{i}\omega_1 t}\,\mathrm{d}\omega_1,$$

where $' = \partial/\partial x$. The form that Y takes in (8) makes it possible to evaluate the partial derivatives with respect to x,

$$\frac{\mathrm{d}^2 y(x,t)}{\mathrm{d}t^2} = -\sum_{n=-\infty}^{\infty}\int_{-\infty}^{\infty}\left[\omega_1^2 - 2v\omega_1\kappa_n + v^2\kappa_n^2\right] \cdot \chi_n(\omega_1)\mathrm{e}^{\mathrm{i}\kappa_n x}\mathrm{e}^{-\mathrm{i}\omega_1 t}\,\mathrm{d}\omega_1,$$

where the parameter $\kappa_n = -k_n + \frac{\omega_1}{v}$; the sum in the parentheses that arose from taking partial derivatives with respect to x and t, however, exactly equals Ω_n^2 ($k_n v = \Omega_n$) independently of ω_1. It is now possible to take the Fourier transform of the excitation force $f(x,t)$, (10),

$$F(x,\omega) = \frac{M_\mathrm{w}}{2\pi v}\sum_{n=-\infty}^{\infty}\Omega_n^2\int_{-\infty}^{\infty}\int_{-\infty}^{\infty}\delta\left(t - \frac{x}{v}\right)\mathrm{e}^{\mathrm{i}(\omega-\omega_1)t}\,\mathrm{d}t \cdot \chi_n(\omega_1)\mathrm{e}^{-\mathrm{i}(k_n - \frac{\omega_1}{v})x}\,\mathrm{d}\omega_1 - \frac{M_\mathrm{w} g}{2\pi v}\int_{-\infty}^{\infty}\delta\left(t - \frac{x}{v}\right)\mathrm{e}^{\mathrm{i}\omega t}\,\mathrm{d}t,$$

where $\delta(x - vt) = \frac{1}{v}\delta(t - x/v)$. Because of the delta function, the integrals in the t variable are easily evaluated,

$$F(x,\omega) = \frac{M_\mathrm{w}}{2\pi v}\sum_{n=-\infty}^{\infty}\Omega_n^2\int_{-\infty}^{\infty}\chi_n(\omega_1)\,\mathrm{d}\omega_1\,\mathrm{e}^{-\mathrm{i}(k_n - \frac{\omega}{v})x} - \frac{M_\mathrm{w} g}{2\pi v}\mathrm{e}^{\mathrm{i}\frac{\omega}{v}x},$$

where the $\mathrm{e}^{\mathrm{i}(\omega_1/v)x}$-factors in the first integral cancel each other out . Together with (13), $F(x,\omega)$ reduces to

$$F(x,\omega) = \frac{M_\mathrm{w}}{2\pi v}\sum_{n=-\infty}^{\infty}\Omega_n^2 x_n\,\mathrm{e}^{-\mathrm{i}(k_n - \frac{\omega}{v})x} - \frac{M_\mathrm{w} g}{2\pi v}\mathrm{e}^{\mathrm{i}\frac{\omega}{v}x}.$$

Generalise for a vehicle with any mass, M_veh, and vertical receptance, α_veh, in the contact point between rail and wheel:

$$F(x,\omega) = \frac{-1}{2\pi v}\sum_{n=-\infty}^{\infty}\alpha_\mathrm{veh}^{-1}(\Omega_n)x_n\,\mathrm{e}^{-\mathrm{i}(k_n - \frac{\omega}{v})x} - \frac{M_\mathrm{veh} g}{2\pi v}\mathrm{e}^{\mathrm{i}\frac{\omega}{v}x}. \quad (14)$$

2.2.2. The Integral Equation

As the wheel (in the preceeding section, Figure 2) traverses the periodically supported rail, it 'sees' a varying receptance downwards, causing a parametric excitation; the response, $y_v(t)$, at the moving point, $x_0 = vt$, is periodic and can be written as a Fourier series, (12), with the unknown coefficients x_n, determined in this section by the infinite system $\boldsymbol{x} = \boldsymbol{A}\boldsymbol{x} + \boldsymbol{b}$ (in matrix form). Four steps remain to reach the goal: (i) calculate $Y(x_0,\omega)$ out of $F(x,\omega)$, (14), by superposition of Green's functions, (1); (ii) take the inverse Fourier transform of $Y(x_0,\omega)$ to obtain $y(x_0,t)$; (iii) put $x_0 = vt$ in $y(x_0,t)$ to get the response of the point moving with the wheel; finally, (iv) discretise the equation by using (5).

First, (14) and (1) imply that

$$Y(x_0,\omega) = \frac{-1}{2\pi v}\sum_{n=-\infty}^{\infty}\alpha_{\text{veh}}^{-1}(\Omega_n)x_n \cdot \int_{-\infty}^{\infty} G_\omega(x|x_0)\mathrm{e}^{-\mathrm{i}(k_n-\frac{\omega}{v})x}\,\mathrm{d}x - \frac{M_{\text{veh}}g}{2\pi v}\int_{-\infty}^{\infty} G_\omega(x|x_0)\mathrm{e}^{\mathrm{i}\frac{\omega}{v}x}\,\mathrm{d}x,$$

or

$$Y(x_0,\omega) = \frac{-1}{2\pi v}\sum_{n=-\infty}^{\infty}\alpha_{\text{veh}}^{-1}(\Omega_n)x_n\hat{G}_\omega\left(k_n-\frac{\omega}{v};x_0\right) - \frac{M_{\text{veh}}g}{2\pi v}\hat{G}_\omega\left(-\frac{\omega}{v};x_0\right),$$

where $\hat{G}$ is defined by (3). The inverse Fourier transform of this is

$$y(x_0,t) = \frac{-1}{2\pi v}\sum_{n=-\infty}^{\infty}\alpha_{\text{veh}}^{-1}(\Omega_n)x_n \cdot \int_{-\infty}^{\infty}\hat{G}_\omega\left(\frac{\Omega_n-\omega}{v};x_0\right)\mathrm{e}^{-\mathrm{i}\omega t}\,\mathrm{d}\omega - \frac{M_{\text{veh}}g}{2\pi v}\int_{-\infty}^{\infty}\hat{G}_\omega\left(-\frac{\omega}{v};x_0\right)\mathrm{e}^{-\mathrm{i}\omega t}\,\mathrm{d}\omega,$$

so that, after having put $x_0 = vt$,

$$y_v(t) = \frac{-1}{2\pi v}\sum_{n=-\infty}^{\infty}\alpha_{\text{veh}}^{-1}(\Omega_n)x_n \cdot \int_{-\infty}^{\infty}\hat{G}_\omega\left(\frac{\Omega_n-\omega}{v};vt\right)\mathrm{e}^{-\mathrm{i}\omega t}\,\mathrm{d}\omega - \frac{M_{\text{veh}}g}{2\pi v}\int_{-\infty}^{\infty}\hat{G}_\omega\left(-\frac{\omega}{v};vt\right)\mathrm{e}^{-\mathrm{i}\omega t}\,\mathrm{d}\omega.$$

Equation (5), with $\omega_0 = \Omega_n$ and $\omega_0 = 0$ respectively, implies that the last expression can be rewritten

$$y_v(t) = -\sum_{n=-\infty}^{\infty}\alpha_{\text{veh}}^{-1}(\Omega_n)x_n\sum_{j=-\infty}^{\infty}a_j(\Omega_n)\mathrm{e}^{-\mathrm{i}(\Omega_n+\Omega_j)t} - M_{\text{veh}}g\sum_{n=-\infty}^{\infty}a_n(0)\mathrm{e}^{-\mathrm{i}\Omega_n t},$$

or

$$\sum_{m=-\infty}^{\infty}x_m\mathrm{e}^{-\mathrm{i}\Omega_m t} = -\sum_{n=-\infty}^{\infty}\sum_{j=-\infty}^{\infty}a_j(\Omega_n)\mathrm{e}^{-\mathrm{i}\Omega_{n+j}t}\alpha_{\text{veh}}^{-1}(\Omega_n)x_n - M_{\text{veh}}g\sum_{n=-\infty}^{\infty}a_n(0)\mathrm{e}^{-\mathrm{i}\Omega_n t},$$

since $y_v(t) = \sum_{m=-\infty}^{\infty}x_m\mathrm{e}^{-\mathrm{i}\Omega_m t}$, (12). After a Fourier transform,

$$\sum_{m=-\infty}^{\infty}x_m\delta(\omega-\Omega_m) = -\sum_{n=-\infty}^{\infty}\sum_{j=-\infty}^{\infty}a_j(\Omega_n)\alpha_{\text{veh}}^{-1}(\Omega_n)x_n\delta(\omega-\Omega_{n+j}) - M_{\text{veh}}g\sum_{n=-\infty}^{\infty}a_n(0)\delta(\omega-\Omega_n).$$

Integrating left and right hand side over Ω_m, i.e. $\int_{\Omega_m-\epsilon}^{\Omega_m+\epsilon}\ldots\mathrm{d}\omega$ and letting $\epsilon\to 0$, implies that

$$x_m = -\sum_{n=-\infty}^{\infty}a_{m-n}(\Omega_n)\alpha_{\text{veh}}^{-1}(\Omega_n)x_n - M_{\text{veh}}g\,a_m(0).$$

The infinite system

$$\boldsymbol{x} = \boldsymbol{A}\boldsymbol{x} + \boldsymbol{b}, \tag{15}$$

couples the response at one frequency, e.g. the fundamental frequency, to the response at all the other harmonics; $\boldsymbol{x}$ and $\boldsymbol{b}$ are infinite vectors, and $\boldsymbol{A}$ is a doubly infinite matrix.

The system (15) may, after truncation, be solved by Gaussian elimination, having rewritten it as $(\boldsymbol{A}-\boldsymbol{I})\boldsymbol{x} = -\boldsymbol{b}$, where $\boldsymbol{I}$ is the identity matrix, provided none of $\boldsymbol{A}$'s eigenvalues equals 1, $\lambda_n \neq 1$; or iteratively, with the scheme $\boldsymbol{x}^{k+1} = \boldsymbol{A}\boldsymbol{x}^k + \boldsymbol{b}$, where the 'initial guess' $\boldsymbol{x}^0 = \boldsymbol{b}$. For convergence of the iteration, $\boldsymbol{A}$'s norm must be less than 1, $||\boldsymbol{A}|| < 1$. The inhomogeneity $\boldsymbol{b}$ of the matrix equation, corresponding to the gravity term of the force, (10), is the 'driving force' of the system, because if $\boldsymbol{b}$ were zero, then $\boldsymbol{x}^0, \boldsymbol{x}^1, \boldsymbol{x}^2, \ldots, \boldsymbol{x}^{k+1} = \boldsymbol{0}$, so $\boldsymbol{x} = \boldsymbol{0}$ would be a solution. Having calculated the solution vector $\boldsymbol{x}$, then for the existence of a solution in the time domain, (12), the Fourier coefficients must decay rapidly enough, according to Parseval's formula. Otherwise, the energy of the solution becomes infinite.

If the vehicle is modelled as a rigid mass only, instability is determined by the following two factors: $M_{\text{w}}v^2/2$, i.e. the translatory kinetic energy of the wheel in the horizontal direction; as well as the degree of receptance variation. Nevertheless, for instability the speed v and mass M_{w} must be much greater than those actually occurring [17].

As mentioned before (Sec. 2.1.2), only the three Fourier coefficients a_0 and $a_{\pm 1}$ of the receptance variation need to

ACUSTICA · acta acustica
Vol. 84 (1998)

be considered in the frequency range 0–2000 Hz, because of rapid decay. Only the three coefficients x_0 and $x_{\pm 1}$ may then be sufficient to describe the solution $y_v(t)$, so (12) changes to

$$y_v(t) = \sum_{n=-1}^{1} x_n e^{-i\Omega_n t},$$

with a constant part, x_0, and a time varying part with coefficients $x_{\pm 1}$. The real part of the variation is

$$\Re\left(\sum_{n=\pm 1} x_n e^{-i\Omega_n t}\right) = 2|x_1|\cos\left[\Omega_1 t + \arg(x_1)\right], \quad (16)$$

where

$$x_1 \simeq \frac{-M_{\text{veh}} g\, a_1(0)}{1 + a_0(\Omega_1)/\alpha_{\text{veh}}(\Omega_1)}, \quad (17)$$

after a simplification of (15).

2.3. Modulation Excitation

2.3.1. Contact Force

Rail receptance variation not only causes a low-frequency excitation at the sleeper-passing circular frequency Ω_1 (with harmonics), but also a modulation of the high-frequency contact force due to rail/wheel surface roughnesses. For an excitation by a moving harmonic point force, with velocity v and circular frequency ω_0, and with an amplitude distribution $F_0(x, \omega_0)$, the Fourier transform of the force, (2), modifies to

$$F(x, \omega) = \frac{1}{2\pi v} e^{-i\frac{\omega_0 - \omega}{v}x} F_0(x, \omega_0). \quad (18)$$

The amplitude of the contact force F_0 between rail and wheel depends on the velocity v, the amplitude r_0 and wavelength λ_0 of the surface roughness (Figure 3). At the circular frequency $\omega_0 = 2\pi v/\lambda_0$,

$$F_0(x, \omega_0) = \frac{-k_{\text{H}} r_0}{1 + k_{\text{H}}(\alpha_{\text{r}} + \alpha_{\text{w}})}, \quad (19)$$

which is a result from dynamic force equilibrium between rail and wheel, assuming a sinusoidal surface profile and a force proportional to the amplitude of the roughness, see also [18, 19, 20]. The vertical point receptance of the rail $\alpha_{\text{r}}(\omega_0) = G_{\omega_0}(x|x)$ is periodic with the sleeper distance l; $\alpha_{\text{w}}(\omega_0)$ is the radial point receptance of the wheel. The linearised Hertzian contact spring k_{H} is determined by formulae readily available [21, 19, 22].

F_0 can be expanded as a Fourier series, $F_0(x, \omega_0) = \sum_{n=-\infty}^{\infty} b_n(\omega_0) e^{ik_n x}$, since α_{r} is periodic with the period l, where the coefficients

$$b_n(\omega_0) = \frac{1}{l}\int_0^l F_0(x, \omega_0) e^{-ik_n x} dx, \quad (20)$$

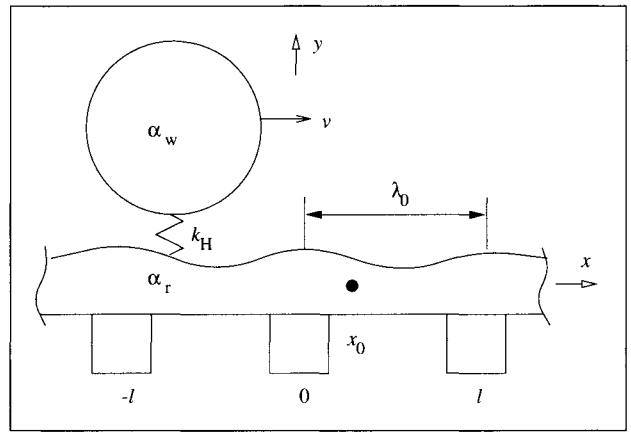

Figure 3. Excitation by surface roughnesses.

and $k_n = 2\pi n/l$. The contact force induces a vertical displacement into the rail and wheel, with Fourier coefficients for the rail

$$c_n(\omega_0) = \frac{1}{l}\int_0^l G_{\omega_0}(x|x) F_0(x, \omega_0) e^{-ik_n x} dx, \quad (21)$$

and for the wheel

$$d_n(\omega_0) = \alpha_{\text{w}}(\omega_0) \cdot \frac{1}{l}\int_0^l F_0(x, \omega_0) e^{-ik_n x} dx. \quad (22)$$

2.3.2. Frequency Spectra

The response of the rail to excitation by the force defined by (18) and (20) results from a superposition of Green's functions, (1):

$$\begin{aligned} Y(x_0, \omega) &= \frac{1}{2\pi v}\sum_{n=-\infty}^{\infty} b_n(\omega_0) \\ &\quad \int_{-\infty}^{\infty} G_\omega(x|x_0) e^{-i\frac{\omega_0 - \omega}{v}x} e^{ik_n x} dx \quad (23) \\ &= \frac{1}{2\pi v}\sum_{n=-\infty}^{\infty} b_n(\omega_0)\hat{G}_\omega\left(\frac{\omega_0 - \omega - \Omega_n}{v}; x_0\right), \end{aligned}$$

where $\hat{G}_\omega$ is defined by (3). The energy of the transient response at a fixed point x_0 of the rail for a wheel passage is $2\pi\int_{-\infty}^{\infty}|Y(x_0, \omega)|^2 d\omega$, according to Parseval. The Doppler shift causes the response to be smeared out around the excitation frequency ω_0. The integral is thus a function of velocity v of the wheel. In practice, however, it is sufficient to calculate the limit of the integral as $v \to 0$ (see Sec. 2.1.2), since the minimum bending wave speed is much faster than any train. Accordingly, it is shown in Appendix A2 that

$$\lim_{v\to 0}\int_{-\infty}^{\infty}|Y(x_0, \omega)|^2 d\omega = \frac{1}{2\pi v}\sum_{n=-\infty}^{\infty}|b_n(\omega_0)|^2\int_{-\infty}^{\infty}|G_{\omega_0 - \Omega_n}(x|x_0)|^2 dx,$$

where G is the Green's function of the rail as defined in the companion paper [16], b_n is the Fourier coefficients

of the contact force between rail and wheel, (20), and $\Omega_n = 2\pi v n/l$ is the fundamental frequency ($n = 1$) with harmonics of the modulation caused by the periodicity. The received energy is caused by excitation at circular frequency ω_0. So, the energy spectrum density (ESD) with respect to ω_0 at point x_0 of the rail is

$$S_{YY}(x_0, \omega_0) = \frac{1}{v} \sum_{n=-\infty}^{\infty} |b_n(\omega_0)|^2 \cdot \int_{-\infty}^{\infty} |G_{\omega_0 - \Omega_n}(x|x_0)|^2 \, \mathrm{d}x. \quad (24)$$

Corresponding formulae for the vertical rail-wheel response at the (forward moving) contact point, are, for the rail

$$S_{Y_v Y_v,\mathrm{R}}(\omega_0) = \sum_{n=-\infty}^{\infty} |c_n(\omega_0)|^2, \quad (25)$$

and for the wheel

$$S_{Y_v Y_v,\mathrm{W}}(\omega_0) = \sum_{n=-\infty}^{\infty} |d_n(\omega_0)|^2. \quad (26)$$

At the contact point, the response is not transient, but periodic, so $S_{Y_v Y_v,\mathrm{R}}$ and $S_{Y_v Y_v,\mathrm{W}}$ are power spectrum densities (PSD). These formulae (24–26) take account of the total energy corresponding to the excitation frequency ω_0 and modulation, but not how this energy is spread out along the frequency axis; the energy corresponding to the frequency component with index n causes a response at the frequency $\omega_0 - \Omega_n$, and not at ω_0 as it appears above. Information regarding the Doppler effect is also lost in the approximate formula (24).

3. Numerical Simulations

3.1. 'Roughness' Excitation Comparison

When all supports and the distances between them are equal, the thesis [12] concludes that only the fundamental, $\Omega_1 = 2\pi f_s = 2\pi v/l$ needs to be considered, due to rapid decay of the harmonics. For very low velocities, equation (17) yields that the response (at the fundamental) $x_1 \simeq -M_{\mathrm{veh}} g \, a_1(0)$, since the track ($a_0$) behaves as a spring and the vehicle (α_{veh}) as a mass at low frequencies. $M_{\mathrm{veh}} g$ is the static load under the actual wheel as 'felt' by the track, while $a_1(0)$ is the static receptance variation of the track. For parameters according to Table I the receptance varies as shown by Figure 4, approximately represented by $G_0(x|x) \simeq a_0(0) + 2a_1(0)\cos k_1 x = a_0(0) + a_{-1}(0)\mathrm{e}^{-\mathrm{i}k_1 x} + a_1(0)\mathrm{e}^{\mathrm{i}k_1 x}$, where $a_1(0) \simeq -82.5 \cdot 10^{-12}$ m/N, or about 2 % of the average, $a_0(0)$ [$a_{-1}(0) = a_1(0)$, since real]. A load $M_{\mathrm{veh}} g$ of 100 kN would then cause a vertical wheel displacement, (16), $2|x_1|$ of 16.5 μm (peak), at very low velocities (frequencies).

Deviations from perfect geometries, e.g. plane rail surfaces, always exist, causing excitations which might reduce the significance of parametric excitation. Smooth rails have roughness amplitudes of the order of μm per third octave band, in the frequency range of interest. If the rail has a 'corrugation' with wavelength λ_0 and amplitude r_0 where the wheel traverses the rail with velocity v, then the vertical dynamic contact force, exciting rail and wheel at the frequency $f_0 = v/\lambda_0$ is [see (19)]

$$F_0 = \frac{-k_{\mathrm{H}} r_0}{1 + k_{\mathrm{H}}(\alpha_{\mathrm{r}} + \alpha_{\mathrm{w}})}.$$

This force induces a vertical displacement into wheel and rail, depending on the relative magnitudes and phases of their receptances. For low frequencies, $|\alpha_{\mathrm{H}}| = |1/k_{\mathrm{H}}| \ll |\alpha_{\mathrm{r}}|, |\alpha_{\mathrm{w}}|$, so the displacement of the rail

$$Y_{\mathrm{r}} \simeq \frac{-r_0}{1 + \alpha_{\mathrm{w}}/\alpha_{\mathrm{r}}},$$

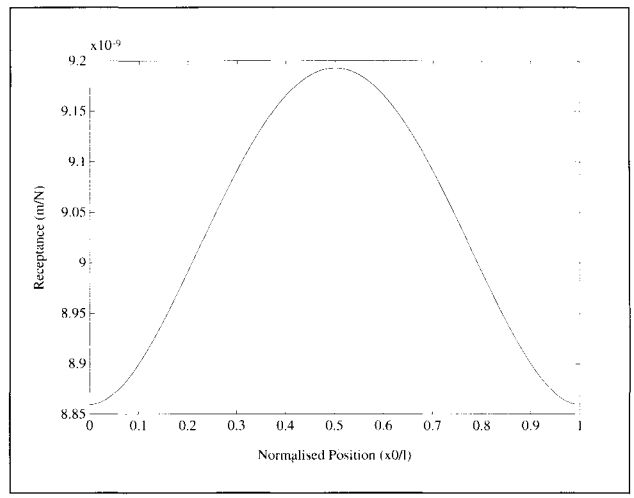

Figure 4. Receptance variation through a sleeper span for rail with stiff pads, $K_{\mathrm{r}} = 500$ MN/m, for a static load, $f_0 = 0$ Hz.

Table I. Track parameters for calculations (see the companion paper [16]).

	Value	Description
E	$2.1 \cdot 10^{11}$ N/m^2	rail modulus of elasticity
η	0.004	rail loss factor
I	$15.45 \cdot 10^{-6}$ m^4	rail moment of aerea inertia
m_{r}	52 kg/m	rail mass per length
l	0.65 m	sleeper spacing
K_{r}	$500 \cdot 10^6$ N/m	pad stiffness
η_{pad}	0.15	pad loss factor
l_{s}	2.5 m	sleeper length
M_{s}	250 kg	sleeper mass
M'_{s}	100 kg/m	sleeper mass per length
B_{s}	$4.6 \cdot 10^6$ Nm^2	sleeper bending stiffness
η_{s}	0.01	sleeper loss factor
K'_{s}	$60 \cdot 10^6$ N/m^2	ballast stiffness per length
C'_{s}	$60 \cdot 10^3$ Ns/m^2	ballast damping per length
z_0	-0.75 m	sleeper excitation point

ACUSTICA · acta acustica
Vol. 84 (1998)

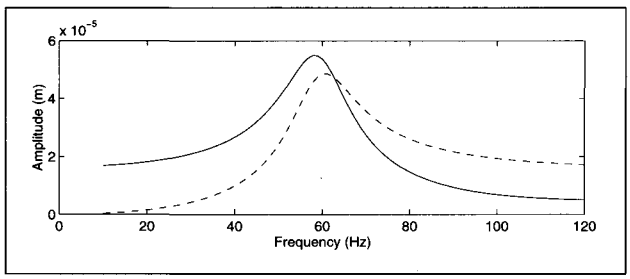

Figure 5. Vertical wheel, Y_w *(solid line)*, and rail, Y_r *(dashed line)*, vibrations caused by a wave form on the rail surface with wavelength $\lambda_0 = l = 0.65$ m (l is the sleeper spacing) and amplitude $r_0 = 16.5$ μm, as a function of the frequency $f_0 = v/\lambda_0$.

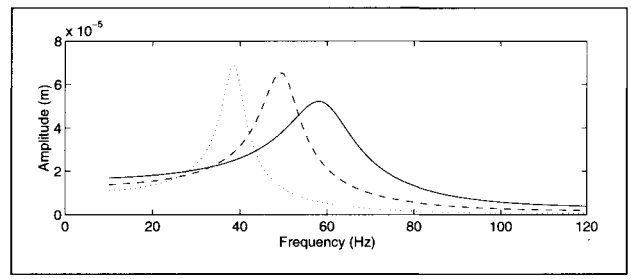

Figure 6. Parametric excitation with different pad stiffnesses, normal ballast ($K'_s = 60$ MN/m^2 and $C'_s = 60$ kNs/m^2): *solid line*, $K_r = 500$ MN/m; *dashed line*, $K_r = 60$ MN/m; *dotted line*, $K_r = 20$ MN/m.

and the wheel

$$Y_w \simeq \frac{r_0}{1 + \alpha_r/\alpha_w}.$$

It is interesting to note that the last expression equals (17), if (i) $r_0 = |-M_{veh} g a_1(0)|$, the static deflection variation caused by the varying rail receptance and the weight of the vehicle; (ii) $\alpha_r(\omega) = a_0(\omega)$, the average rail receptance through a sleeper span; and (iii) the wheel receptance $\alpha_w(\omega) = \alpha_{veh}(\omega)$; in the current low frequency region $\alpha_{veh} \simeq \alpha_w \simeq -1/M_w\omega^2$.

To estimate the importance of parametric excitation, vertical vibrations induced into rail and wheel by a wave form on the rail surface with a wavelength of $\lambda_0 = l = 0.65$ m (l is sleeper spacing) and an amplitude of $r_0 = 16.5$ μm are plotted (Figure 5). The wheel receptance is assumed as a rigid mass of 600 kg. Rail vibrations, Y_r, equal wheel vibrations, Y_w, around the ballast resonance, 60 Hz. Below the ballast resonance $|Y_r| < |Y_w|$; otherwise $|Y_r| > |Y_w|$. The response of the wheel equals that caused by parametric excitation, according to the discussion above. Below ballast resonance, however, the rail response due to 'corrugation' is less than the wheel response, and hence also less than the response caused by parametric excitation. Thus, if the rail has a 'corrugation' with the same wavelength and amplitude as the static deflection variation through a sleeper span, parametric excitation is the dominant rail vibration source below ballast resonance.

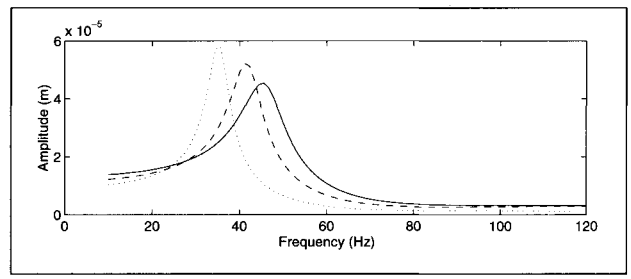

Figure 7. Parametric excitation with different pad stiffnesses, soft ballast ($K'_s = 30$ MN/m^2 and $C'_s = 30$ kNs/m^2): *solid line*, $K_r = 500$ MN/m; *dashed line*, $K_r = 60$ MN/m; *dotted line*, $K_r = 20$ MN/m.

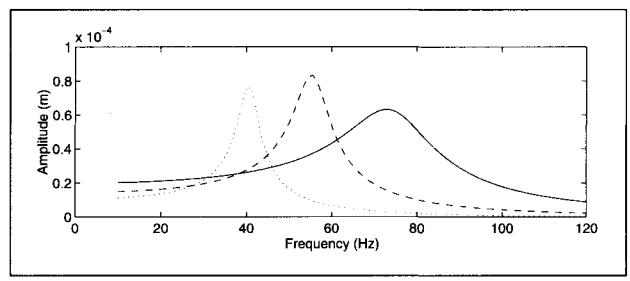

Figure 8. Parametric excitation with different pad stiffnesses, stiff ballast ($K'_s = 120$ MN/m^2 and $C'_s = 120$ kNs/m^2): *solid line*, $K_r = 500$ MN/m; *dashed line*, $K_r = 60$ MN/m; *dotted line*, $K_r = 20$ MN/m.

3.2. Track Design Optimisation

Numerical simulations of parametrically excited vibrations are performed assuming a rigid mass (600 kg) wheel with vehicle preload 100 kN. Track data are the same as in Table I, unless otherwise stated. All curves display wheel/rail response at the sleeper-passing frequency $f_s = v/l$ as a function of this frequency.

The general behaviour of the response curves (Figures 6–12) is that of a mass-spring-damper system, with the resonance frequency somewhere between 30–80 Hz, depending on track and vehicle parameters. A softer pad (Figures 6–8), or ballast (Figure 9), moves this resonance downwards. At the same time, the vibration level decreases, except around

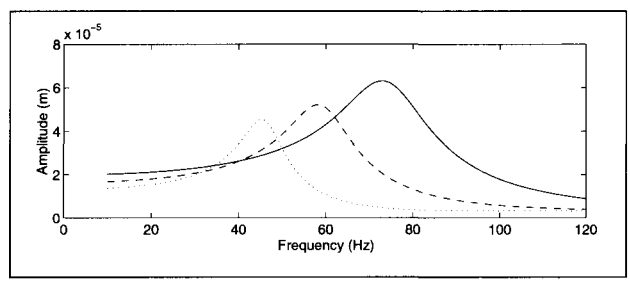

Figure 9. Parametric excitation with different ballast properties: *solid line*, $K'_s = 120$ MN/m^2 and $C'_s = 120$ kNs/m^2; *dashed line*, $K'_s = 60$ MN/m^2 and $C'_s = 60$ kNs/m^2; *dotted line*, $K'_s = 30$ MN/m^2 and $C'_s = 30$ kNs/m^2.

the new resonance frequency, where it increases; the reduction is striking around the old resonance. Selecting softer pads, reduces the vibration level more if the ballast is stiff

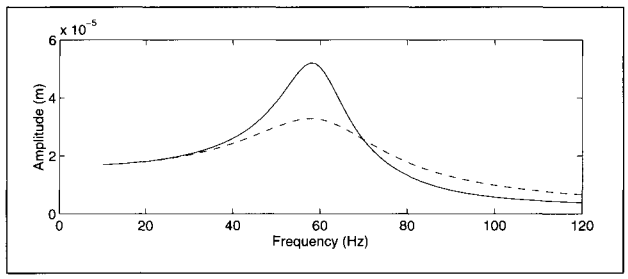

Figure 10. Parametric excitation with different ballast dampings: *solid line*, $C'_s = 60$ kNs/m^2; *dashed line*, $C'_s = 120$ kNs/m^2.

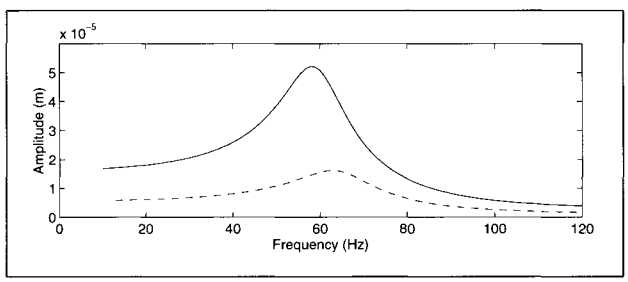

Figure 11. Parametric excitation with different sleeper spacings: *solid line*, $l = 0.65$ m; *dashed line*, $l = 0.5$ m.

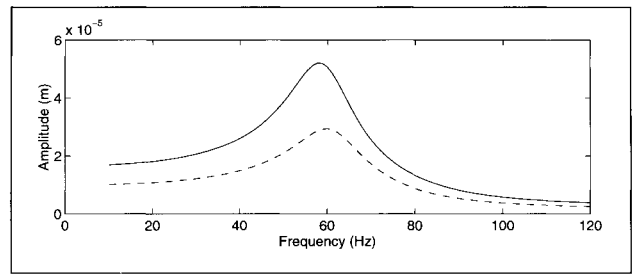

Figure 12. Parametric excitation with different rails: *solid line*, UIC 50; *dashed line*, UIC 60.

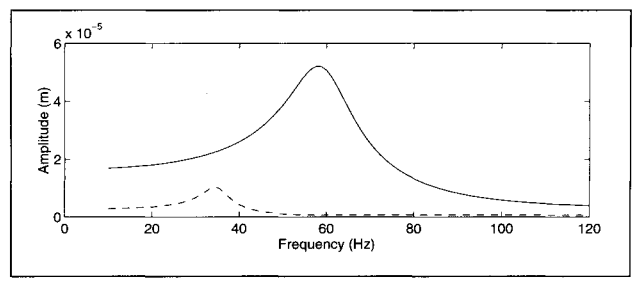

Figure 13. Parametric excitation with different train weights: *solid line*, $P = 100$ kN, $K'_s = 60$ MN/m^2 and $C'_s = 60$ kNs/m^2; *dashed line*, $P = 25$ kN, $K'_s = 15$ MN/m^2 and $C'_s = 15$ kNs/m^2.

(Figure 8). Only increasing ballast damping reduces the vibration level around the resonance (Figure 10), but increases it slightly above.

Introducing more receptance in the track, through pads or ballast, efficiently reduces parametric excitation. For relatively fast trains, say $v > 140$ km/h and $f_s > 60$ Hz, the reduction is achieved by a shift downwards of the vehicle-track resonance, enabling a vibration reduction potential of some 20 dB (see e.g. Figure 9). For very slow trains, $v < 70$ km/h and $f_s < 30$ Hz, however, the reduction potential is only about 3 dB, because now the reduction is not from a resonance shift but one of reduced receptance variation. Altering track elasticity must be done with caution, so that the new resonance frequency does not coincide with the sleeper-passing frequency for trains on that particular line, thus aggravating the vibrational situation.

Figures 11 and 12 show the vibration reduction achieved by shortening the sleeper distance from 0.65 m to 0.5 m; or substituting the rail from UIC 50 to UIC 60, with $m_r = 60$ kg/m and $I = 22.5 \cdot 10^{-6}$ m^4. The rail moment inertia, reduced in the calculation by 25 % from the tabulated value ($30 \cdot 10^{-6}$ m^4) for a UIC 60-rail, for the same reason as in [16]. These measures are particularly efficient, since they work for all speeds and frequencies. Reduced sleeper distance, however, also implies increased sleeper-passing frequency, assuming the speed is held constant.

Parametric excitation increases dramatically with train weight. The curves in Figure 13 may e.g. represent calculated vibrations for main-line traffic (heavy) and for local traffic (light). Decreased preload also implies softer ballast and lower damping (Figure 9 and [12]), taken into account, when comparing light and heavy trains.

3.3. Modulation Excitation

The rail-wheel dynamic contact force, according to (19), is a function of the linearised Hertzian contact spring k_H, the amplitude of the surface roughness r_0, rail receptance α_r and wheel receptance α_w. In the calculations here, the wheel receptance is taken from the measurements described in [12]; rail parameters, defining the rail receptance, are chosen in accordance with Table I.

The received rail vibrational energy at a fixed point, during a wheel passage on a rail with a sinusoidal surface profile, obviously depends on the contact force, but also on speed, (23); the frequency content is a function of speed, v, and wavelength of the surface profile, λ_0, but also on the sleeper distances l through modulation with circular frequencies Ω_n (sleeper-passing frequency with harmonics). In the calculation of Figure 14, the following parameters were used: $v = 220$ km/h, $\lambda_0 = 66$ mm so that the excitation frequency equalled the pinned-pinned frequency, $f_0 = f_{pp} = 927$ Hz; the amplitude of the surface profile $r_0 = 10$ μm. The response spectrum at $x_0/l = 0.5$ has a double-peak, accompanied by smaller double-peaks around the excitation frequency $f_0 = 927$ Hz.

The shape of the curve in Figure 14 is a consequence of a combination of modulation of the contact force and Doppler shift (see also Ripke [5]). Without Doppler shift, there would be one peak at f_0, accompanied by smaller peaks at $f_0 \pm nf_s$ ($n = 1, 2, \ldots$), due to modulation of the force with sleeper-passing frequency $f_s = v/l$. Bringing Doppler effect into the picture, each peak is split into a double peak, where the locations of the two main peaks are approximately at $f_0 \pm v/\lambda_B$ (Sec. 2.1.2). Clearly, a lot of energy is contained

ACUSTICA · acta acustica
Vol. 84 (1998)

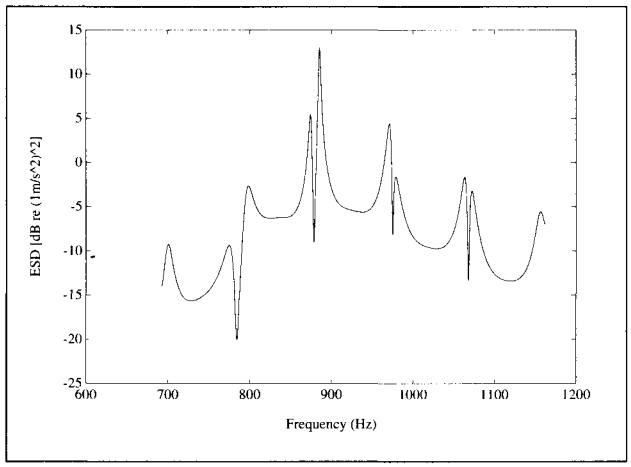

Figure 14. Energy spectrum density (ESD), $|Y(x_0,\omega)|^2$, of rail with sinusoidal surface profile, traversed by a wheel.

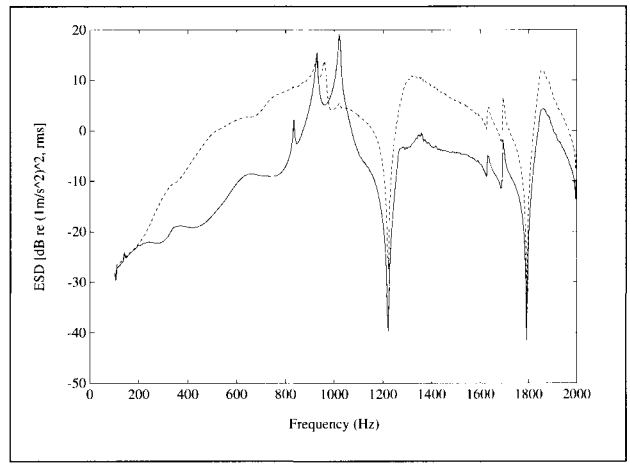

Figure 15. Energy spectrum density (ESD) of the rail, $S_{YY}(x_0,\omega_0)$, at $x_0/l = 0.5$: *solid line*, $K_r = 500$ MN/m; *dashed line*, $K_r = 60$ MN/m.

in the first terms of the modulation, around the pinned-pinned frequency. Neglect of the second terms, however, have little influence on the total energy of the response, more than 10 dB lower than the main peaks.

Figure 15 shows vertical response spectra of rail vibration for a wheel passage at 220 km/h. The surface roughness spectrum density of the rail $\Phi_{r_0r_0}(k_0) \sim k_0^{-1.83}$ m^3, where the roughness wavenumber $k_0 = \omega_0/v = 2\pi/\lambda_0$ [12]. Obviously, the roughness spectrum slopes by some 18 dB/decade. At this speed, filtering effects in the rail/wheel contact region [12] have little effect around/below the pinned-pinned frequency (around 1000 Hz). Apparently, the ESD-levels are generally greater for a rail-sleeper system with soft rather than stiff pads, but not around the pinned-pinned frequency, where the behaviour is more complicated, displaying a greater maximum with stiff than with soft pads.

Vibrations propagate freely through a rail-sleeper system with soft rather than with stiff pads (see companion paper [16]). Validation of the TWINS noise prediction program, emphasises the importance of carefully considering attenuation along the rail [23], which is a great advantage of the current model. What is more, TWINS suggests the use of very stiff pads to minimise noise [24] since this reduces the effective radiating rail length. This effect, however, may be offset to some extent by an increase in noise generation due to increased modulation around the pinned-pinned frequency.

The curve for the rail with stiff pads has three sharp peaks around the pinned-pinned frequency. Without modulation, the energy of the pinned-pinned mode would be underestimated; the peak at $f_{pp} + f_s \simeq 1020$ Hz, due to modulation, carries more energy than the peak at the pinned-pinned frequency (stiff pads). As a result of adopting the limit $v \to 0$, in calculating the response spectrum, (24), the peaks due to the modulation are located at $f_{pp} \pm f_s$ (Figure 15). Yet, calculating the spectrum directly from (23) (no approximation) produces only one great peak at the pinned-pinned frequency, as demonstrated in the thesis [12]. To sum this paragraph, in calculating noise generation from stiffly padded rail, it is important to account for the energy due to modulation.

4. Conclusions

Varying track receptance induces low-frequency ground vibration and compartment noise, increasing linearly with train weight. Coincidence between the sleeper-passing frequency f_s and wheel-ballast resonance, typically 50–100 Hz, results in great amplitudes. Increasing track receptance through pads or ballast, shortening sleeper spacings and/or using a stiffer/heavier rail may reduce parametric excitation. A comparison with 'roughness' (large-scale geometric deviations) excited rail vibrations shows that parametric excitation is dominant below the wheel-ballast resonance, assuming the same 'roughness' amplitude as the static deflection variation. The wheel, however, responds equally to 'roughness' as to parametric excitation, in the low frequency range.

The dynamic contact force caused by short-scale roughnesses fluctuates through the sleeper spans, with stiff pads providing an extra excitation mechanism, which is significant at the pinned-pinned frequency f_{pp}, typically around 1000 Hz. Green's function of the periodically supported rail allows for calculating the received energy spectrum density (ESD) at a fixed rail point during a wheel pass-by, automatically including rail vibration attenuation with length, being important in noise control. Reduced pad stiffness increases the total ESD, but lowers the response around f_{pp}.

Appendix

A1. Spatial Fourier Transform of Green's Function

The spatial Fourier transform in the x direction of Green's function

$$\hat{G}(\kappa; x_0) = \int_{-\infty}^{\infty} G(x|x_0) e^{-i\kappa x} dx.$$

Green's function has been determined in companion paper [16].

Evaluation of the integral results in

$$\hat{G}(\kappa) =$$
$$c_1^{\mathrm{r}}\left[\int_{x_0}^{l} Y_1^{\mathrm{r}} \mathrm{e}^{-\mathrm{i}\kappa x}\mathrm{d}x + \int_0^{l} Y_1^{\mathrm{r}} \mathrm{e}^{-\mathrm{i}\kappa x}\mathrm{d}x \sum_{n=1}^{\infty} \mathrm{e}^{n(g_1^{\mathrm{r}}-\mathrm{i}\kappa l)}\right]$$
$$+ c_2^{\mathrm{r}}\left[\int_{x_0}^{l} Y_2^{\mathrm{r}} \mathrm{e}^{-\mathrm{i}\kappa x}\mathrm{d}x + \int_0^{l} Y_2^{\mathrm{r}} \mathrm{e}^{-\mathrm{i}\kappa x}\mathrm{d}x \sum_{n=1}^{\infty} \mathrm{e}^{n(g_2^{\mathrm{r}}-\mathrm{i}\kappa l)}\right]$$
$$+ c_1^{\mathrm{l}}\left[\int_{0}^{x_0} Y_1^{\mathrm{l}} \mathrm{e}^{-\mathrm{i}\kappa x}\mathrm{d}x + \int_0^{l} Y_1^{\mathrm{l}} \mathrm{e}^{-\mathrm{i}\kappa x}\mathrm{d}x \sum_{n=-1}^{-\infty} \mathrm{e}^{n(g_1^{\mathrm{l}}-\mathrm{i}\kappa l)}\right]$$
$$+ c_2^{\mathrm{r}}\left[\int_{0}^{x_0} Y_2^{\mathrm{l}} \mathrm{e}^{-\mathrm{i}\kappa x}\mathrm{d}x + \int_0^{l} Y_2^{\mathrm{l}} \mathrm{e}^{-\mathrm{i}\kappa x}\mathrm{d}x \sum_{n=-1}^{-\infty} \mathrm{e}^{n(g_2^{\mathrm{l}}-\mathrm{i}\kappa l)}\right].$$

The infinite sums appear using $Y(x+nl)\mathrm{e}^{-\mathrm{i}\kappa(x+nl)} = Y(x)\mathrm{e}^{-\mathrm{i}\kappa x}\mathrm{e}^{n(g-\mathrm{i}\kappa l)}$, thanks to Floquet's theorem, where $Y = Y_{1,2}^{\mathrm{r,l}}$ and $g = g_{1,2}^{\mathrm{r,l}}$, in order to change the integration interval from $]-\infty, +\infty[$ to $[0, l]$. They are easily evaluated as geometric series. Rewriting this expression as

$$\hat{G}(\kappa) = c_1^{\mathrm{r}}\left[I(x_0,l,g_1^{\mathrm{r}}) + I(0,l,g_1^{\mathrm{r}})\frac{\mathrm{e}^{g_1^{\mathrm{r}}-\mathrm{i}\kappa l}}{1-\mathrm{e}^{g_1^{\mathrm{r}}-\mathrm{i}\kappa l}}\right]$$
$$+ c_2^{\mathrm{r}}\left[I(x_0,l,g_2^{\mathrm{r}}) + I(0,l,g_2^{\mathrm{r}})\frac{\mathrm{e}^{g_2^{\mathrm{r}}-\mathrm{i}\kappa l}}{1-\mathrm{e}^{g_2^{\mathrm{r}}-\mathrm{i}\kappa l}}\right]$$
$$+ c_1^{\mathrm{l}}\left[I(0,x_0,g_1^{\mathrm{l}}) + I(0,l,g_1^{\mathrm{l}})\frac{1}{\mathrm{e}^{g_1^{\mathrm{l}}-\mathrm{i}\kappa l}-1}\right]$$
$$+ c_2^{\mathrm{l}}\left[I(0,x_0,g_2^{\mathrm{l}}) + I(0,l,g_2^{\mathrm{l}})\frac{1}{\mathrm{e}^{g_2^{\mathrm{l}}-\mathrm{i}\kappa l}-1}\right]$$

after having introduced the function

$$I(a,b,g_{1,2}^{\mathrm{r,l}}) = \int_a^b Y_{1,2}^{\mathrm{r,l}} \mathrm{e}^{-\mathrm{i}\kappa x}\,\mathrm{d}x.$$

Finally, $I(a,b,g)$ are evaluated, by selecting the homogeneous solutions $Y_{1,2}^{\mathrm{r,l}}$ from [16] [recall that $c = -Y(0)/4$]:

$$Y(x) = \frac{K}{Bk^3}\left[\frac{\sin k(l-x) + \mathrm{e}^g \sin kx}{\cos kl - \cosh g} - \frac{\sinh k(l-x) + \mathrm{e}^g \sinh kx}{\cosh kl - \cosh g}\right]$$

where $Y = Y_{1,2}^{\mathrm{r,l}}$ and $g = g_{1,2}^{\mathrm{r,l}}$. After some calculation,

$$I(a,b,g) =$$
$$\frac{K}{Bk^3}\left\{\left[\mathrm{e}^{-\mathrm{i}\kappa a}\left[k\cos k(l-a) - \mathrm{i}\kappa \sin k(l-a)\right]\right.\right.$$
$$\left. - \mathrm{e}^{-\mathrm{i}\kappa b}\left[k\cos k(l-b) - \mathrm{i}\kappa \sin k(l-b)\right]\right]$$
$$\cdot\left[(\kappa^2-k^2)(\cos kl - \cosh g)\right]^{-1}$$
$$+ \mathrm{e}^g\left[-\mathrm{e}^{-\mathrm{i}\kappa a}\left[k\cos ka + \mathrm{i}\kappa \sin ka\right]\right.$$
$$\left. + \mathrm{e}^{-\mathrm{i}\kappa b}\left[k\cos kb + \mathrm{i}\kappa \sin kb\right]\right]$$
$$\left[(\kappa^2-k^2)(\cos kl - \cosh g)\right]^{-1}$$
$$- \left[\mathrm{e}^{-\mathrm{i}\kappa a}\left[k\cosh k(l-a) - \mathrm{i}\kappa \sinh k(l-a)\right]\right.$$
$$\left. - \mathrm{e}^{-\mathrm{i}\kappa b}\left[k\cosh k(l-b) - \mathrm{i}\kappa \sinh k(l-b)\right]\right]$$
$$\left[(\kappa^2+k^2)(\cosh kl - \cosh g)\right]^{-1}$$
$$- \left[\mathrm{e}^{g}\left[-\mathrm{e}^{-\mathrm{i}\kappa a}\left[k\cosh ka + \mathrm{i}\kappa \sinh ka\right]\right.\right.$$
$$\left.\left. + \mathrm{e}^{-\mathrm{i}\kappa b}\left[k\cosh kb + \mathrm{i}\kappa \sinh kb\right]\right]\right.$$
$$\left.\left[(\kappa^2+k^2)(\cosh kl - \cosh g)\right]^{-1}\right\}.$$

A2. Received Rail Energy from a Moving Harmonic Force

The response of the rail

$$Y(x_0,\omega) = \int_{-\infty}^{\infty} G_\omega(x|x_0)F(x,\omega)\,\mathrm{d}x.$$

The moving harmonic force

$$F(x,\omega) = \frac{1}{2\pi v}\mathrm{e}^{-\mathrm{i}\frac{\omega_0-\omega}{v}x} F_0(x,\omega_0),$$

modulated by the periodic amplitude function $F_0(x+l,\omega) = F_0(x,\omega)$. Thus, F_0 can be expressed as a Fourier series

$$F_0(x,\omega_0) = \sum_{n=-\infty}^{\infty} b_n(\omega_0)\mathrm{e}^{\mathrm{i}k_n x},$$

where $k_n = 2\pi n/l = \Omega_n/v$. According to Parseval, the energy of the response is

$$2\pi\int_{-\infty}^{\infty} |Y(x_0,\omega)|^2\,\mathrm{d}\omega.$$

First, assume that the amplitude function $F_0 = 1$. By inserting the expressions for Y and F, above, the integral becomes

$$\int_{-\infty}^{\infty} |Y(x_0,\omega)|^2\,\mathrm{d}\omega =$$
$$\frac{1}{(2\pi v)^2}\int_{-\infty}^{\infty}\int_{-\infty}^{\infty}\int_{-\infty}^{\infty} G_\omega^*(x|x_0)\mathrm{e}^{\mathrm{i}\frac{\omega_0-\omega}{v}x}$$
$$\cdot G_\omega(x'|x_0)\mathrm{e}^{-\mathrm{i}\frac{\omega_0-\omega}{v}x'}\,\mathrm{d}x\,\mathrm{d}x'\,\mathrm{d}\omega,$$

where * denotes complex conjugate. Since

$$\hat{G}_\omega(\kappa;x_0) = \int_{-\infty}^{\infty} G_\omega(x|x_0)\mathrm{e}^{-\mathrm{i}\kappa x}\mathrm{d}x.$$

where $\kappa = (\omega_0-\omega)/v$ [see equation (3)],

$$\int_{-\infty}^{\infty} |Y(x_0,\omega)|^2\,\mathrm{d}\omega = \frac{1}{(2\pi v)^2}\int_{-\infty}^{\infty} \hat{G}_\omega^*\left(\frac{\omega_0-\omega}{v};x_0\right)$$
$$\cdot \hat{G}_\omega\left(\frac{\omega_0-\omega}{v};x_0\right)\mathrm{d}\omega.$$

ACUSTICA · acta acustica
Vol. 84 (1998)

When $v \to 0$, the order of $\lim_{v\to 0}$ and $\int$ may be interchanged, because $\hat{G} \to 0$ rapidly as $\kappa \to \pm\infty$ [$\hat{G} = \mathcal{O}(\kappa^{-4})$ as $\kappa \to \pm\infty$ since $G_\omega^{(iv)}(x|x_0)$ is absolutely integrable, except for a few isolated step discontinuities of $G_\omega'''(x|x_0)$]. Therefore, in the new integration variable κ,

$$\lim_{v\to 0} \int_{-\infty}^{\infty} |Y(x_0,\omega)|^2 \,\mathrm{d}\omega = \frac{1}{v(2\pi)^2} \int_{-\infty}^{\infty} \hat{G}^*_{\omega_0}(\kappa; x_0)\hat{G}_{\omega_0}(\kappa; x_0) \,\mathrm{d}\kappa.$$

Use the definition of $\hat{G}_\omega(\kappa; x_0)$:

$$\lim_{v\to 0} \int_{-\infty}^{\infty} |Y(x_0,\omega)|^2 \,\mathrm{d}\omega = \frac{1}{v(2\pi)^2} \int_{-\infty}^{\infty}\int_{-\infty}^{\infty}\int_{-\infty}^{\infty} G^*_{\omega_0}(x'|x_0) \cdot G_{\omega_0}(x|x_0)\mathrm{e}^{\mathrm{i}\kappa(x'-x)} \,\mathrm{d}x \,\mathrm{d}x' \,\mathrm{d}\kappa.$$

The κ-integral becomes $2\pi\delta(x'-x)$, easing the integration in the x'-variable, so that finally

$$\lim_{v\to 0} \int_{-\infty}^{\infty} |Y(x_0,\omega)|^2 \,\mathrm{d}\omega = \frac{1}{2\pi v} \int_{-\infty}^{\infty} |G_{\omega_0}(x|x_0)|^2 \,\mathrm{d}x.$$

It is now easy to show, similarly as above, that for a general periodic amplitude function F_0,

$$\lim_{v\to 0} \int_{-\infty}^{\infty} |Y(x_0,\omega)|^2 \,\mathrm{d}\omega = \frac{1}{2\pi v} \sum_{n=-\infty}^{\infty} |b_n(\omega_0)|^2 \int_{-\infty}^{\infty} |G_{\omega_0-\Omega_n}(x|x_0)|^2 \,\mathrm{d}x.$$

Acknowledgement

Swedish Transport & Communications Research Board (KFB) supported the project, running January '90 – June '95. Thanks are also due to all my colleagues at The Marcus Wallenberg Laboratory for Sound and Vibration Research; and at Institut für Technische Akustik, Technische Universität Berlin.

With special thanks to Professor Anders Nilsson, MWL.

References

[1] R. Wettschureck, G. Hauck: Geräusche und Erschütterungen aus dem Schienenverkehr. – In: Taschenbuch der Technischen Akustik. M. Heckl, H. Müller (eds.). Springer-Verlag, 1994, Kap. 16.

[2] L. Auersch: Zur Parametererregung des Rad-Schienen-Systems: Berechnung der Fahrzeug-Fahrweg-Untergrund-Dynamik und experimentelle Verifikation am Hochgeschwindigkeitszug Intercity Experimental. Ingenieur-Archiv **60** (1990) 141–156.

[3] L. Cremer, M. Heckl: Körperschall. Second ed. Springer-Verlag, 1996, 2., völlig neubearbeitete Auflage.

[4] M. Heckl: The role of the sleeper-passing frequency in rail-wheel noise. Transport Noise '94, October 1994. The East-European Acoustical Association. 109–116. Held in St. Petersburg, Russia.

[5] B. Ripke: Hochfrequente gleismodellierung und simulation der fahrzeug-gleis-dynamik unter verwendung einer nichtlinearen kontaktmechanik. Dissertation. Technische Universität Berlin, 1994. Fortschritt-Berichte VDI Reihe 12 Nr. 249.

[6] L. Frýba: Vibration of solids and structures under moving loads. Noordhoff International Publishing, Groningen, 1972.

[7] K. Knothe, S. L. Grassie: Modelling of railway track and vehicle/track interaction at high frequencies. Vehicle System Dynamics **22** (1993) 209–262.

[8] S. Timoshenko: Method of analysis of statical and dynamical stresses in rail. Proceedings of the Second International Congress for Applied Mechanics, Zürich, 1926. 407–418.

[9] C. E. Inglis: The vertical path of a wheel moving along a railway track. Journal of the Institution of Civil Engineers **11** (1939) 262–288.

[10] J. Dörr: Der unendliche, federnd gebettete Balken unter dem Einfluß einer gleichförmig bewegten Last. Ingenieur-Archiv **14** (1943) 167–192.

[11] J. Dörr: Das Schwingungsverhalten eines federnd gebetteten, unendlich langen Balkens. Ingenieur-Archiv **16** (1948) 287–298.

[12] A. Nordborg: Vertical Rail Vibrations: Noise and Structure-Borne Sound Generation. Dissertation. Kungl Tekniska Högskolan, Stockholm, 1995.

[13] A. Nordborg: Vertikale Schwingungen einer Schiene beim Abrollen eines Rades. DAGA 94 - Dresden, March 1994.

[14] H. Ilias, K. Knothe: Ein diskret kontinuierliches Gleismodell unter Einfluß schnell bewegter, harmonisch schwankender Wanderlasten. Tech. Rept. Reihe 12 Nr. 171, Fortschritt-Berichte VDI, VDI-Verlag GmbH, Düsseldorf, 1992.

[15] J. Kisilowski, Z. Strzyżakowski, B. Sowiński: Application of discrete-continuous model systems in investigating dynamics of wheelset-track system vibrations. ZAMM—Z. angew. Math. Mech. **68** (1988) T70–T71.

[16] A. Nordborg: Vertical Rail Vibrations: Pointforce Excitation. ACUSTICA — acta acustica **84** (1997) 280–288.

[17] M. A. Heckl: Flutter-like instabilities caused by feedback in the rail-wheel interaction. A Workshop on Rolling Noise Generation, October 1989. Institute für Technische Akustik, Technische Universität Berlin. 112–117.

[18] S. L. Grassie, R. W. Gregory, D. Harrison, K. L. Johnson: The dynamic response of railway track to high frequency vertical excitation. Journal Mechanical Engineering Science **24** (1982) 77–90.

[19] P. J. Remington: Wheel/rail rolling noise, I: Theoretical analysis. Journal of the Acoustical Society of America **81** (1987) 1805–1823.

[20] D. J. Thompson: Wheel-rail noise generation, part I: Introduction and interaction model. Journal of Sound and Vibration **161** (1993) 387–400.

[21] J. Feldmann: A theoretical model for structure-borne excitation of a beam and ring in rolling contact. Journal of Sound and Vibration **116** (1987) 527–543.

[22] D. J. Thompson: Wheel-rail noise generation, part IV: Contact zone and results. Journal of Sound and Vibration **161** (1993) 447–466.

[23] D. J. Thompson, P. Fodiman, H. Mahé: Experimantal validation of the TWINS prediction program for rolling noise, part 2: results. Journal of Sound and Vibration **193** (1996) 137–147.

[24] N. Vincent, P. Bouvet, D. J. Thompson, P. E. Gautier: Theoretical optimization of track components to reduce rolling noise. Journal of Sound and Vibration **193** (1996) 161–171.